ARTICLES

High-pressure fluorescence line narrowing of Eu(III)-doped sodium disilicate glass

Michael J. Lochhead and Kevin L. Bray*
Department of Chemical Engineering, University of Wisconsin–Madison, Madison, Wisconsin 53706
(Received 3 August 1995)

High-pressure fluorescence line narrowing (HPFLN) has been used to characterize the local structure of Eu^{3+} ions in sodium disilicate glass up to 210 kbar. HPFLN spectra, measured at 77 K, were analyzed using crystal-field theory. As pressure was increased from ambient to approximately 40 kbar, a redshift of the $^5D_0 \leftarrow {}^7F_0$ excitation band was accompanied by a simultaneous decrease in the Eu^{3+} site crystal-field strength and a lengthening of the fluorescence lifetime from approximately 2.3 to 2.4 ms. These trends were reversed above 40 kbar, as crystal-field strength increased with pressure and lifetime decreased linearly to approximately 1.4 ms at 210 kbar. The $^5D_0 \leftarrow {}^7F_0$ excitation band broadened significantly above 70 kbar and continued to shift red above 150 kbar. HPFLN results are interpreted in terms of structural changes in the silicate glass matrix and compression of the Eu^{3+} bonding environment. Lifetime and intensity changes are attributed to a pressure-induced increase in the electron-phonon coupling to local vibrations. Pressure-induced crystal-field effects are used to deduce characteristics of high- and low-crystal-field-strength sites in ambient pressure glasses. Spectral and lifetime results for the sample released from high pressure show that a new local Eu^{3+} structure is formed during decompression.

I. INTRODUCTION

Inorganic glasses doped with rare-earth or transition-metal ions continue to be an important class of optical materials. Although the luminescence properties of these materials depend intimately on the local structure of the dopant ions, elucidation of this structure remains challenging. The lack of periodicity of structure in glass limits the applicability of conventional x-ray-diffraction techniques. Newer techniques, including extended x-ray-absorption fine structure (EXAFS) and neutron scattering, have been successfully used to obtain information about average bond lengths and coordination numbers. Ideally, however, site-specific structural information for the dopant is desired.

Optical spectroscopic methods allow one to probe the local environments of dopant ions in a glass. Among these methods, fluorescence line narrowing (FLN) spectroscopy has proved useful for obtaining local structure information.[1] The disordered structure of the glass leads to site-to-site variations in the local bonding and electronic energy levels of dopants and a consequent inhomogeneous broadening of spectral features. In FLN spectroscopy, the inhomogeneous broadening is suppressed by using a laser excitation source with a linewidth that is much narrower than an absorption band of the dopant. Only dopant ions in sites that permit absorption resonant with the laser are excited. As a consequence, the resulting fluorescence spectrum is greatly simplified and ideally represents the contribution from one or a small number of distinct bonding sites. Tuning of the excitation source over the entire inhomogeneous absorption band permits the sampling of all bonding sites. Crystal-field analysis of FLN spectra can be used to develop quantitative parameters related to the local structure. These parameters can then be used to analyze geometrical models of the ensemble of bonding environments occupied by a dopant in a glass. In practice, accidental degeneracy, phonon-assisted absorption, and energy transfer can complicate the interpretation of FLN spectra.[1] These topics are discussed in detail in the text.

In addition to providing the local structural information useful for modeling and predicting the technological optical properties of doped glasses, FLN spectroscopy can be used to probe structural transformations that occur in glass. Durville *et al.*[2] and Capobianco *et al.*,[3] for example, have used FLN spectroscopy to probe nucleation of crystalline phases in glasses to produce glass ceramics.

The theme of our work is to use high pressure to systematically alter the local structure of luminescent dopants in insulating crystalline and glassy materials. The basic effect of compression is to reduce the volume of the material through distortions of bond lengths and bond angles. Our goals are to relate local structure to optical properties and to develop optical methods for probing pressure-induced structural transformations.

Previous high-pressure optical studies of crystalline materials have shown that pressure generally leads to an increase in dopant crystal-field strength and an enhancement of the nephelauxetic effect.[4–8] These effects have been exploited to assist in assigning spectral transitions, to deduce local symmetry and to resolve overlapping spectral features. Much of the recent work has emphasized level crossing in Cr^{3+}-doped crystals[9–14] and covalency and crystal-field effects in a variety of transition metal[15–18] and rare-earth-doped crystals,[19–24] including those doped with Eu^{3+}.[5,6,25–29] In addition, Chen *et al.* demonstrated amorphization of $Eu(OH)_3$ at high pressure using Eu^{3+} fluorescence spectroscopy.[30]

High-pressure optical studies of transition-metal- or rare-

0163-1829/95/52(22)/15763(13)/$06.00

earth-doped glasses are far less common due to the more complicated nature of these systems. The optical absorption studies by Tischer of Cr^{3+}-doped glasses up to 50 kbar indicated that Cr^{3+} adopts a nearly regular octahedral bonding configuration in oxide glasses and that crystal-field strength and covalency both increase with pressure.[31] Tischer and Drickamer also reported tetrahedral-to-octahedral conversions of Co^{2+} and Ni^{2+} in silicate and phosphate glasses at high pressure.[32] More recently, Soga *et al.* used Eu^{3+} fluorescence to study densification effects in borate glasses quenched from high temperatures and pressures.[33]

In a context independent of the optical materials characterization described above, geologists have long been interested in the effects of pressure on the phases, structures, and bonding of minerals, melts, and glasses. The interest has been prompted by a desire to understand the processes that occur at the high-temperature and high-pressure conditions that prevail in the Earth's interior. A variety of techniques, including infrared[34,35] and Raman spectroscopies,[35–38] NMR,[39–42] and diffraction techniques,[43,44] have been applied *in situ* at high pressure or on pressure-quenched samples. Although the majority of work has considered undoped systems, a number of studies focusing on optical absorption of transition metals in naturally occurring or synthetic analogs of geological materials has been reported.[45–48] These studies have considered the effects of pressure on coordination number, crystal-field strength, cation partitioning, bulk modulus, and phase stability. An important finding from the studies of undoped silica and alkali or alkaline-earth-modified silicates is the ability of pressure to increase the coordination number of Si from 4 to 5 and 6.[37,39,41,49–51]

In this paper we describe an experiment, high-pressure fluorescence line narrowing (HPFLN) spectroscopy for studying the high-pressure properties of glass. The experiment combines the site-selective potential of FLN spectroscopy with *in situ* high-pressure characterization. Our goal is to develop a fluorescence-based probe of pressure-induced changes in glass structure and at the same time to correlate these changes with optical properties of luminescent dopants in an effort to develop structure-property relations for optical glasses.

We report the results of HPFLN studies of sodium disilicate (Na_2O-$2SiO_2$) glass using Eu^{3+} as the fluorescent probe. Eu^{3+} was selected because its nondegenerate $^5D_0 \leftarrow {}^7F_0$ transition is ideally suited for FLN analysis.[1] Sodium disilicate glass serves as a model composition from both the optical materials and geological minerals perspectives. We found a decrease in the Eu^{3+}-site crystal-field strength up to ~40 kbar followed by an increase in field strength up to 210 kbar. The changes in crystal-field strength were accompanied by an increase in fluorescence lifetime up to ~40 kbar followed by a decrease. The increased width of the $^5D_0 \leftarrow {}^7F_0$ band of Eu^{3+} with pressure indicates that Eu^{3+} occupies a wider range of structural sites at high pressure. Spectra obtained on release of pressure indicate an irreversible distortion of the Eu^{3+} bonding environment. These effects are discussed in terms of likely pressure-induced structural rearrangements and coordination changes.

II. EXPERIMENT

A. Sample preparation

The Eu^{3+}-glass sample (molar composition $0.94Eu_2O_3$-$32.86Na_2O$-$66.15SiO_2$) was prepared in a manner similar to that used by Cormier *et al.*[52] Appropriate amounts of Eu_2O_3, Na_2CO_3, and amorphous SiO_2 (Aldrich) were ground together using mortar and pestle. The powder was placed in a platinum crucible and melted at 1300 °C for 1 h in an ambient atmosphere box furnace. The melt was quenched in de-ionized water, recrushed, and remelted to ensure homogeneity. The glass product was annealed at 500 °C for 1 h.

B. Diamond anvil cell

Large hydrostatic pressures were generated using a modified Merrill-Bassett diamond anvil cell (DAC), custom built by Eifle, Inc. Low-fluorescence diamonds with a culet diameter of approximately 0.7 mm were used. The sample chamber consisted of a 250-μm hole drilled in a pre-indented Inconel gasket. Small pieces of the glass sample (characteristic dimension 100 μm) were loaded in the sample chamber along with the ruby chips used as the pressure calibrant.[53] A 4:1 methanol:ethanol solution was used as the pressure fluid.[54] The methanol:ethanol fluid remains hydrostatic to 104 kbar, above which small nonisotropic stresses may develop. Nonisotropic stresses can be detected by broadening of the ruby R lines used in the pressure calibration. No significant nonhydrostatic effects were detected over the pressure range encountered in this study. Pressure was increased at room temperature, and the DAC was allowed to equilibrate for at least 1 h at each pressure step. Spectroscopic measurements were carried out at 77 K by submerging the DAC in liquid nitrogen.

C. Laser spectroscopy

The laser spectroscopy apparatus consisted of a Q-switched Nd:YAG laser (Continuum NY-61) pumping a tunable dye laser (Spectra-Physics PDL-3). The dye was a 60:40 mixture of rhodamine 590 and rhodamine 560 (Exciton, Inc.). The dye laser pulse duration was approximately 10 ns and had a width of approximately 0.1 cm^{-1}. This system showed low-amplified spontaneous emission in the tuning range of this study (570–583 nm).

The DAC was submerged in a custom-built liquid nitrogen Dewar equipped with quartz windows (Cryo Industries). Fluorescence was collected in front-face mode and focused on the entrance slit of a 1-m monochromator (SPEX 1704). A slit width of 300 μm was used in the FLN experiments, yielding a band pass of approximately 0.24 nm at 600 nm. The detector was a cooled Hamamatsu 2228 photomultiplier tube (PMT). A PMT signal was sent to a fast preamplifier, followed by an amplifier discriminator and photon counter (EG&G ORTEC 9301, 9302, and 934, respectively). Alternatively, time-resolved FLN spectra were collected by sending the PMT signal directly to a Stanford Research Systems boxcar integrator (SR250) which allowed control of the sampling gate delay and width. Scans were performed using software developed in house. This apparatus was also used to generate $^5D_0 \leftarrow {}^7F_0$ excitation spectra by fixing the detection system near the peak of the $^5D_0 \rightarrow {}^7F_2$ emission and then scanning the dye laser across the absorption band.

Fluorescence decay measurements were performed by sending the PMT signal directly to a digital storage oscilloscope (LeCroy ScopeStation 140) equipped with 10 kΩ load

resistor. Decays were measured for different excitation wavelengths by monitoring $^5D_0 \rightarrow {}^7F_2$ emission at 612 nm. Because of the weak signals associated with the diamond cell, it was necessary to detect the strongest part of the fluorescence spectrum in all cases, and wide slits (2 mm, 1.6 nm bandpass) were used. Consequently, our results represent an overall decay time at each pressure. Decays were slightly nonexponential in all cases. Lifetimes were calculated in two ways. First, a single-exponential fit of the slightly nonexponential data was performed. Second, the integrated area of the normalized decay curves was calculated. The methods yielded similar lifetimes and showed identical trends. The integrated areas are reported here.

III. CRYSTAL-FIELD ANALYSIS

A. Theory

Crystal-field theory and its application to rare-earth ions has been described in detail by Wybourne[55] and reviewed by Morrison and Leavitt.[56] Crystal-field theory treats ions of the host matrix as point charges in space and assumes that interactions between the rare-earth ion and its ligands are purely electrostatic. Bond covalency terms are neglected, and neither the spatial extent of the electron clouds nor orbital overlap is formally considered. With these assumptions the electrostatic crystal-field Hamiltonian can be written:

$$H_{\mathrm{CF}} = \sum_{km} B_{km}(r) C_{km}(\theta,\phi). \tag{1}$$

The angular $C_{km}(\theta,\phi)$ spherical tensors are directly related to the spherical harmonics $Y_{km}(\theta,\phi)$ and can be calculated analytically.[55] The radial B_{km} terms are the crystal-field parameters and are normally treated as empirical quantities calculated using experimental energy levels and a fitting procedure. Crystal-field parameters can be predicted from theory using the relation $B_{km} = A_{km}\langle r^k \rangle (1-\sigma_k)$,[56] where $\langle r^k \rangle$ are related to the radial wave functions, σ_k is a correction factor accounting for the shielding effects of outerlying $5s^2$ and $5p^6$ electrons and A_{km} are the crystal-field components, defined as[56]

$$A_{km} = -\frac{e^2}{4\pi\varepsilon_0} \sum_j Z_j \frac{C_{km}(\theta_j,\phi_j)}{R_j^{k+1}}. \tag{2}$$

The sum is over all ligands in a glass or all ions in a host lattice. Z_j is the magnitude of each point charge, and R_j is the radial distance from the rare-earth ion to point charge j. It should be noted that because of the uncertainty in the determination of the radial wave functions, theoretical calculations of the crystal-field parameters are at best approximate.[56]

Symmetry of the rare-earth-ion bonding sites is used to simplify the crystal-field Hamiltonian. Lempicki *et al.* have derived energy equations and crystal-field matrix elements using the operator-equivalent method for Eu^{3+} in a number of site symmetries, neglecting the effects of J mixing.[57] The crystal-field analysis in this work is based on the equations of Lempicki *et al.* for C_{2v} symmetry. C_{2v} is the highest symmetry that allows complete splitting of all crystal-field components, and it has been used extensively in the crystal-field analysis of Eu^{3+} in oxide glasses. Arguments for selecting C_{2v} symmetry have been described by Brecher and Riseberg.[58] The relationship between the operator equivalents and spherical-tensor crystal-field parameters is described by Morrison and Leavitt.[56]

The fact that J mixing is neglected in our analysis should be addressed. J mixing refers to the mixing of M_J components of electronic states with different J values by the crystal-field potential. J mixing has often been neglected in crystal-field analyses of Eu^{3+} energy levels, primarily because of the large separation ($\sim$12 000 cm^{-1}) between the ground-state manifold (^7F_J) and the first excited state ($^5D_0$).[59] Energy-level calculations with and without J mixing in Eu^{3+} crystals have shown that reasonable results can be obtained when J mixing is neglected.[59] J mixing has a more serious effect on the calculation of the transition intensities. We leave J mixing as a future refinement of our analysis. By neglecting J mixing in this paper, we allow direct comparison of our high-pressure results with the large body of previous work in which J mixing is neglected as an approximation.

B. Determining energy levels from FLN spectra

Simple crystal-field analysis of Eu^{3+} bonding requires knowledge of the energies of the three Stark components of the $^7F_1$ state and the five components of the $^7F_2$ state relative to the ground-state energy. The energies are commonly determined by fitting the $^5D_0 \rightarrow {}^7F_{1,2}$ FLN spectra with the appropriate number of Gaussian line-shape functions. This method was used in our analysis using commercial nonlinear least-squares-fitting software.

Several studies have pointed out the presence of a broadband background beneath the line-narrowed spectra of Eu^{3+} oxide glasses.[58,60] Belliveau and Simkin attribute the background to nonresonant excitation of Eu^{3+} ions resulting from a phonon-assisted absorption process.[60] We believe energy transfer may also contribute to the broadband background, particularly in our glass, which has a relatively high dopant concentration (0.94 mol % Eu_2O_3).

We have corrected for the energy transfer or phonon-assisted absorption broadband background beneath the $^5D_0 \rightarrow {}^7F_1$ band in the manner described in detail by Belliveau and Simkin.[60] The method involves using additional Gaussian bands to account for the broadband background, particularly when the high-energy side of the $^5D_0 \leftarrow {}^7F_0$ transition is excited. Although a broadband background beneath the $^5D_0 \rightarrow {}^7F_1$ bands implies a similar effect associated with the $^5D_0 \rightarrow {}^7F_2$ transition, we have not attempted to correct this band and performed the $^5D_0 \rightarrow {}^7F_2$ fits with five Gaussians in all cases. The overlap of the Stark components in the $^5D_0 \rightarrow {}^7F_2$ band leads to a degree of arbitrariness in the fitting of these energy levels. In order to produce a consistent set of energy levels at pressure, positions of the five $^5D_0 \rightarrow {}^7F_2$ bands of the previous pressure were used as the initial values in the Gaussian fits. Using additional Gaussians to fit this band only increased the arbitrariness, and we found no physical justification for using more than five bands. This was especially true for the high-pressure FLN spectra, where significant $^5D_0 \rightarrow {}^7F_2$ structure is lost. Consequently, ambiguity exists in our fitted energies of the high-pressure $^5D_0 \rightarrow {}^7F_2$ Stark components. This ambiguity resulted in in-

creased uncertainty in the crystal-field parameters, particularly those of rank $k=4$ (B_{40}, B_{42}, and B_{44}).

C. Crystal-field parameter and strength calculations

The crystal-field parameters were calculated using the operator-equivalent-derived equations of Lempicki *et al.*[57] for C_{2v} symmetry ($J=1$ and 2 components only) and the eight experimental energy levels determined from the FLN spectra. A fitting procedure based on a simplex algorithm was used to estimate the crystal-field parameters.[3] The accuracy of the fitting procedure was confirmed by successfully reproducing fitted energy levels reported in the literature.[3,60]

Methods for estimating the overall scalar crystal-field strength (S_{CF}) were developed by Auzel[61,62] and Leavitt.[63] The functional form used here is[64]

$$S_{CF}=\left\{\frac{1}{3}\sum_{k}\frac{1}{2k+1}\left[B_{k0}^2+2\sum_{m>0}(\mathrm{Re}\,B_{km}^2+\mathrm{Im}\,B_{km}^2)\right]\right\}^{1/2}. \tag{3}$$

Because of the expected uncertainties in our B_{4m} parameters, we have found it useful to also calculate the $k=2$ contribution to the overall crystal-field strength separately:

$$S_{CF}^{(2)}=\left\{\frac{1}{3}\left[\frac{1}{5}(B_{20}^2+2B_{22}^2)\right]\right\}^{1/2}. \tag{4}$$

$S_{CF}^{(2)}$ is a parameter that quantifies the overall crystal-field strength based primarily on the crystal-field-induced splitting of the $^5D_0\rightarrow{}^7F_1$ transition. A similar procedure was used by Dexpert-Ghys *et al.* to quantify overall crystal-field strength in Eu^{3+}-doped aluminoborosilicate glass.[65] We note that in order to allow comparison of S_{CF} and $S_{CF}^{(2)}$ to values presented in recent studies,[52] we converted the operator-equivalent B_{km} parameter values to the spherical tensor values[56] prior to the S_{CF} calculations.

IV. RESULTS

A. Ambient-pressure FLN spectra and crystal-field calculations

Figure 1 illustrates a representative set of FLN spectra collected at ambient pressure and 77 K at a gate delay of 100 μs. Collecting the spectra at the short gate delay was performed to minimize energy-transfer effects. Despite the 100-μs gate delay, evidence of energy transfer and phonon-assisted absorption was still present in the spectra as seen in the nonresonant $^5D_0\rightarrow{}^7F_0$ emission near 580 nm. The resultant broadband background was accounted for during the Gaussian fitting procedure as described above.

Table I lists the crystal-field parameters calculated from the FLN spectra using the operator-equivalent equations of Lempicki *et al.* for C_{2v} symmetry.[57] Also listed are the strength parameters S_{CF} and $S_{CF}^{(2)}$. Both S_{CF} and $S_{CF}^{(2)}$ decreased as the excitation wavelength was lengthened.

Lifetime measurements were performed for a series of excitation wavelengths while monitoring emission at the peak of the $^5D_0\rightarrow{}^7F_2$ band near 612 nm. A slight lengthening of the lifetime with increasing excitation wavelength was observed, which is consistent with the general trend observed by Brecher and Riseberg.[58] We did not correct for the broadband background in the lifetime measurements, which explains why the lifetime trend observed here was less significant than that observed by those authors.

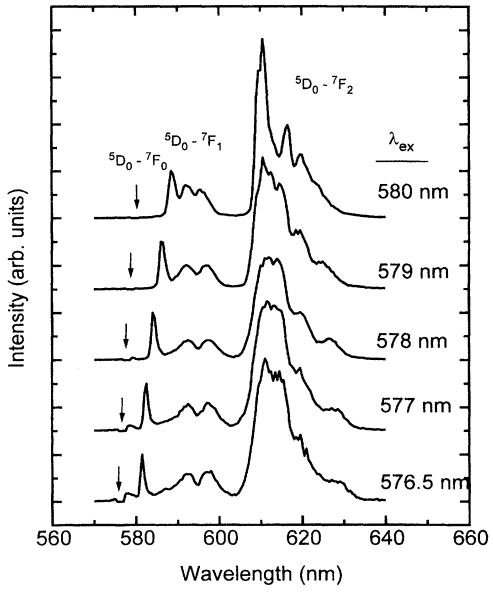

FIG. 1. Eu^{3+}:sodium disilicate glass FLN spectra at atmospheric pressure and 77 K. Spectra were collected during a 15-μs gate at a delay of 100 μs after the laser excitation pulse. Excitation wavelength is indicated at the right of each spectrum and with a small vertical arrow. Spectra are normalized to the $^5D_0\rightarrow{}^7F_1$ peak intensity.

B. HPFLN spectra and crystal-field calculations

Three separate pressure runs were performed and FLN spectra were measured at a total of 18 different pressures. Over 160 spectra were collected for this sample. Representative sets of HPFLN spectra are provided in Figs. 2 and 3 at 66 and 210 kbar, respectively. The fluorescence signal was weak and sensitive to the sample–pump-beam alignment due to the small sample size ($\sim$100 μm) used with the diamond cell. Alignment, therefore, had to be carefully optimized at each pressure. Because of the weakness of the fluorescence signal, it was impossible to perform the time-resolved, short-gate-delay measurements, and so the spectra were collected in a photon counting mode. Consequently, the HPFLN spectra represent all of the photons emitted over a 3-s counting time and necessarily contain any long-time energy-transfer effects. In addition, the range of wavelengths used to excite the sample at each pressure was determined by the signal strength.

In addition to any alignment and sample size effects, an actual decrease in the overall fluorescence intensity was observed as the pressure was increased. Factors explaining the intensity decrease are addressed later. It can be noted here that the loss of intensity was reversible, as the signal strength returned when the pressure was released.

The effect of pressure on the $^5D_0\leftarrow{}^7F_0$ transition was assessed by measuring excitation spectra as a function of pressure. The results are summarized in Fig. 4, where the

TABLE I. Crystal-field parameters at atmospheric pressure.[a]

Pressure (kbar)	λ_{ex} (nm)	B_{20} (cm^{-1})	B_{22} (cm^{-1})	B_{40} (cm^{-1})	B_{42} (cm^{-1})	B_{44} (cm^{-1})	S_{CF} (cm^{-1})	$S_{CF}^{(2)}$ (cm^{-1})	Lifetime (±0.05 ms)
atm	576	−714	376	−94	984	−539	535	385	2.15
	576.5	−673	412	−111	987	−584	533	369	
	577	−619	418	−110	995	−460	515	343	2.11
	577.5	−585	432	−118	1006	−409	512	329	
	578	−543	406	−119	1014	−322	500	305	2.15
	578.5	−479	410	−111	1012	−259	477	276	
	579	−414	404	−121	1013	−85	465	245	2.28
	579.5	−342	367	−112	1076	83	459	208	
	580	−252	327	−115	1113	247	453	163	2.32
	580.5	−192	211	−96	1037	348	405	117	

[a]λ_{ex} is the laser excitation wavelength. B_{km} are the operator-equivalent-derived crystal-field parameters based on Lempicki's equations for C_{2v} symmetry. S_{CF} and $S_{CF}^{(2)}$ are the overall crystal-field strength parameters defined in Eqs. (3) and (4) and were computed after converting the listed B_{km} to their spherical tensor values (Ref. 56). Lifetime values correspond to the integrated area of the normalized decay curves.

horizontal lines represent the full width of the band at half peak intensity and the symbols represent the approximate peak maxima. An initial redshift of approximately 0.012 nm/kbar was observed as the pressure was increased from 0 to ~47 kbar. The peak position then remained largely unchanged between 47 and 130 kbar. A further small redshift was observed as the pressure was increased above 130 kbar. The bandwidth remained unchanged up to approximately 70 kbar, followed by increased broadening at higher pressures.

In order to compare spectra and parameters at different pressures, we felt it was necessary to follow the shift in the $^5D_0 \leftarrow {}^7F_0$ band. We have attempted to follow the same set of "sites" during compression by comparing spectra corresponding to the same region in the shifting $^5D_0 \leftarrow {}^7F_0$ band. In Fig. 5, for example, the HPFLN spectra approximately correspond to excitation of the peak of the $^5D_0 \leftarrow {}^7F_0$ band. The excitation wavelength is listed with each spectrum. As can be seen in Fig. 5, compression gradually leads to increased crystal-field splittings, increased linewidths, and the loss of structure, particularly in the $^5D_0 \rightarrow {}^7F_2$ band.

Crystal-field parameters were calculated for all excitation wavelengths at all pressures. Representative results are presented in Table II. Also listed are calculations of the overall crystal-field strengths S_{CF} and $S_{CF}^{(2)}$ and the fluorescence lifetimes. The overall crystal-field strength parameter $S_{CF}^{(2)}$ is plotted versus excitation wavelength for a series of pressures

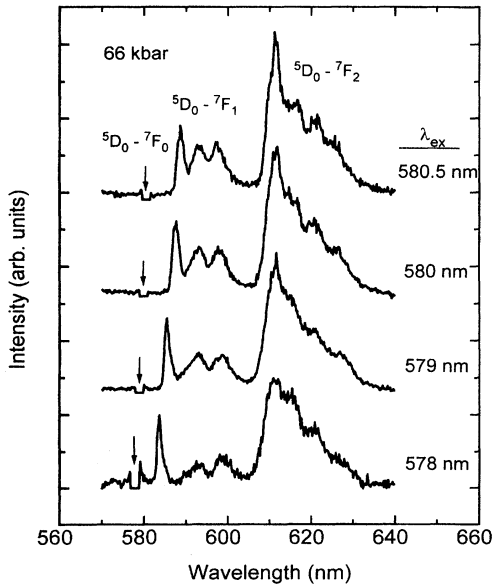

FIG. 2. Eu^{3+}:sodium disilicate glass HPFLN spectra at 66 kbar and 77 K. The excitation wavelength is indicated at the right of each spectrum and with a small vertical arrow. Spectra are normalized to the $^5D_0 \rightarrow {}^7F_1$ peak intensity.

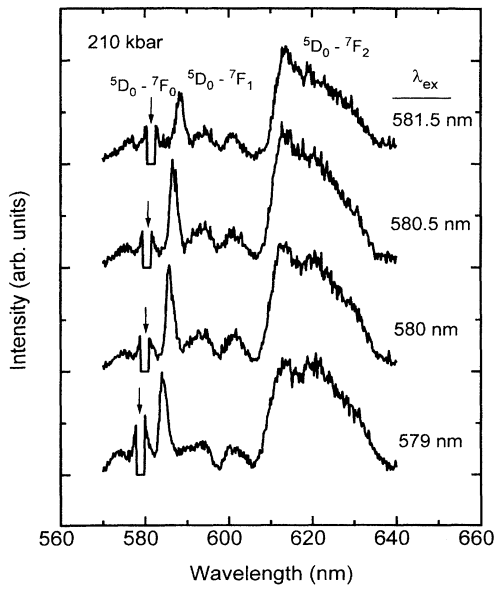

FIG. 3. Eu^{3+}:sodium disilicate glass HPFLN spectra at 210 kbar and 77 K. The excitation wavelength is indicated at the right of each spectrum and with a small vertical arrow. Spectra are normalized to the $^5D_0 \rightarrow {}^7F_1$ peak intensity.

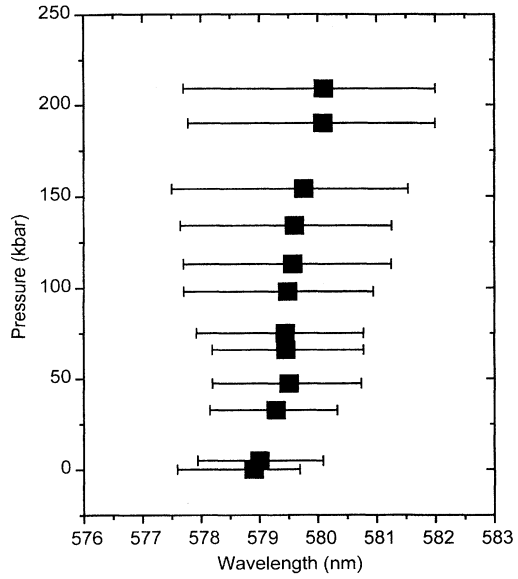

FIG. 4. Peak position (■) and full width at half maximum (length bar) of the $^5D_0 \leftarrow {}^7F_0$ excitation spectra of Eu^{3+}:sodium disilicate glass at 77 K. Excitation spectra were measured by scanning the dye laser across the $^5D_0 \leftarrow {}^7F_0$ band while monitoring $^5D_0 \rightarrow {}^7F_2$ emission at 612 nm. Uncertainties are approximately ±0.2 nm.

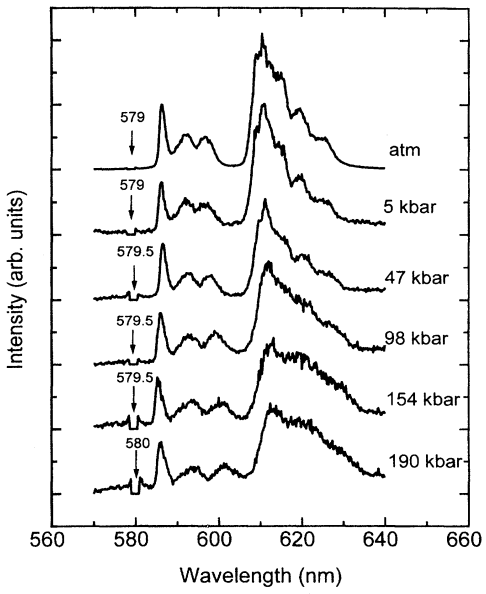

FIG. 5. Eu^{3+}:sodium disilicate glass HPFLN during compression at 77 K. Excitation wavelength is indicated at the right of each spectrum and with a small vertical arrow, and corresponds to the approximate peak intensity of the $^5D_0 \leftarrow {}^7F_0$ band. Spectra are normalized to the $^5D_0 \rightarrow {}^7F_1$ peak intensity.

in Fig. 6. $S_{CF}^{(2)}$ parameters corresponding to the peak of the $^5D_0 \leftarrow {}^7F_0$ band are plotted in Fig. 7. The major observation in Fig. 7 is that as the pressure was increased to ~40 kbar, a decrease in the overall field strength was observed, followed by a field-strength increase as pressure was increased above 40 kbar. The same trend was observed when corresponding regions of the $^5D_0 \leftarrow {}^7F_0$ band were excited during the pressure experiments, suggesting that all sites undergo a decrease followed by an increase in crystal-field strength with pressure.

Pressure had a significant effect on the $^5D_0$ state lifetime. Representative results are listed in Table II and are illustrated in Fig. 8. The lifetimes roughly correspond to excitation near the peak of the $^5D_0 \leftarrow {}^7F_0$ band in each case. We observed an initial increase in the lifetime from ~2.3 ms at ambient pressure to ~2.4 ms at 40 kbar. This was followed by a gradual, approximately linear (−0.0063 ms/kbar) decrease in the lifetime as the pressure was increased from 35 to 210 kbar. The lifetime at 210 kbar for 580-nm excitation was ~1.4 ms.

C. Pressure release

Fluorescence spectra on pressure release indicated that some irreversible structural change took place during the pressurization-release cycle. After pressure release, the sample was allowed to relax for 24 h at room temperature prior to the fluorescence measurements. Room-temperature broadband spectra and representative 77-K FLN spectra are compared for the sample before and after pressurization in Fig. 9. The most obvious difference in the spectra was the increased relative intensity of the hypersensitive $^5D_0 \rightarrow {}^7F_2$ emission for the sample pressurized to 210 kbar. The spectra in Fig. 9 indicate that a permanent distortion towards increased asymmetry of the Eu^{3+} bonding sites took place during the pressurization-release cycle. In addition to the relative intensity changes, the lifetimes of the sample released from high pressure were significantly shorter than those prior to compression (Table II).

A return of fluorescence intensity was also observed on pressure release. As discussed above, the overall fluorescence signal decreased with increased compression. The intensity effect was reversible, and the signal from the released sample was similar to that prior to pressurization.

V. DISCUSSION

FLN studies provide a means of investigating variations in the local bonding environment of Eu^{3+} ions in inorganic glasses. In this discussion, Eu^{3+}-site crystal-field strengths, $^5D_0 \leftarrow {}^7F_0$ band energies, and $^5D_0$ state fluorescence lifetimes are used to develop a description of the local Eu^{3+} bonding environment in silicate glasses. In addition, pressure-induced changes in FLN spectra and structural parameters are used to improve our understanding of local structure in both the high-pressure and ambient-pressure glasses.

The ability to develop unique local structure models using FLN spectra has been called into question by a number of researchers.[52,66] In particular, recent simulation studies have shown that accidental degeneracy may be more significant than previously considered, with multiple local Eu^{3+} bonding geometries yielding the same $^5D_0 \leftarrow {}^7F_0$ energy.[52] We do not propose unique structural models based on our HPFLN results. Rather, we provide a qualitative description of the high- and low-field-strength sites in silicates that we believe is consistent with a variety of experimental data.

TABLE II. Representative crystal-field parameters at high pressure.[a]

Pressure (kbar)	λ_{ex} (nm)	B_{20} (cm^{-1})	B_{22} (cm^{-1})	B_{40} (cm^{-1})	B_{42} (cm^{-1})	B_{44} (cm^{-1})	S_{CF} (cm^{-1})	$S_{CF}^{(2)}$ (cm^{-1})	Lifetime (±0.05 ms)
33	577	−639	417	−98	1104	−437	542	353	
	578	−558	450	−126	1088	−233	529	318	2.40
	579	−440	440	−126	1093	−124	498	262	2.43
	580	−302	340	−112	1067	211	447	186	2.50
66	578	−594	491	−120	1060	−268	532	340	
	579	−501	497	−140	1117	−151	532	298	2.31
	580	−374	449	−137	1129	81	501	235	2.34
134	578	−630	466	−119	1285	−141	596	354	
	579	−593	506	−120	1287	−2	581	327	1.83
	580	−471	487	−130	1298	96	566	283	1.78
	581	−378	340	−108	1105	476	472	220	
210	579	−615	543	−114	1310	−23	601	356	
	580	−545	540	−128	1156	−109	550	324	1.38
	581	−483	536	−137	1131	−108	532	296	1.43
atm	577	−612	393	−110	1123	−276	541	337	1.51
(release)	578	−522	423	−111	1068	−274	504	298	1.59
	579	−412	419	−117	1037	−118	470	247	1.66
	580	−294	381	−131	1050	159	455	190	1.50

[a]λ_{ex} is the laser excitation wavelength. B_{km} are the operator-equivalent-derived crystal-field parameters based on Lempicki's equations for C_{2v} symmetry. S_{CF} and $S_{CF}^{(2)}$ are the overall crystal-field parameters defined in Eqs. (3) and (4) and were computed after converting the listed B_{km} to their spherical tensor values (Ref. 56). Lifetime values correspond to the integrated area of the normalized decay curves.

A. Ambient-pressure FLN

The ambient-pressure FLN studies of the Eu^{3+}-doped sodium disilicate glass yielded results consistent with previous studies of Eu^{3+} ions in silicate glasses.[3,58,60] In addition to the characteristic oxide glass FLN spectra, the derived crystal-field parameters and field-strength calculations (Table I) are similar to literature results. Despite the similarity of various oxide glass FLN spectra and parameters, no strong consensus exists on the nature of the local structure around Eu^{3+}.

Cormier *et al.*[52] have suggested that no individual structural factor greatly influences the electronic spectra of doped

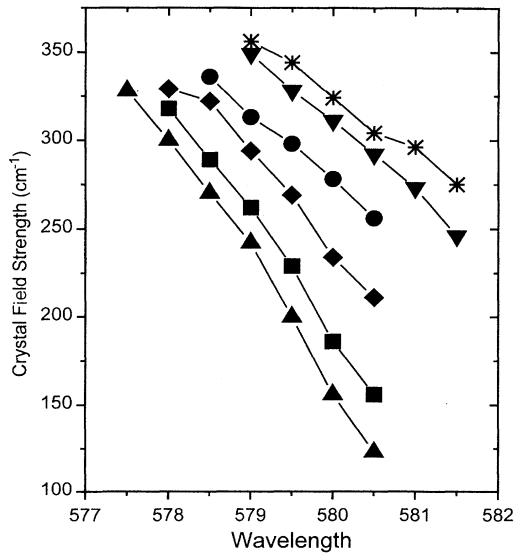

FIG. 6. Overall scalar crystal-field strength $S_{CF}^{(2)}$ [Eq. (4)] as a function of $^5D_0 \leftarrow {}^7F_0$ excitation wavelength. ▲, atmospheric pressure; ■, 33 kbar; ◆, 75 kbar; ●, 113 kbar; ▼, 190 kbar; *, 210 kbar. Uncertainties (not indicated) are approximately ±15 cm^{-1}.

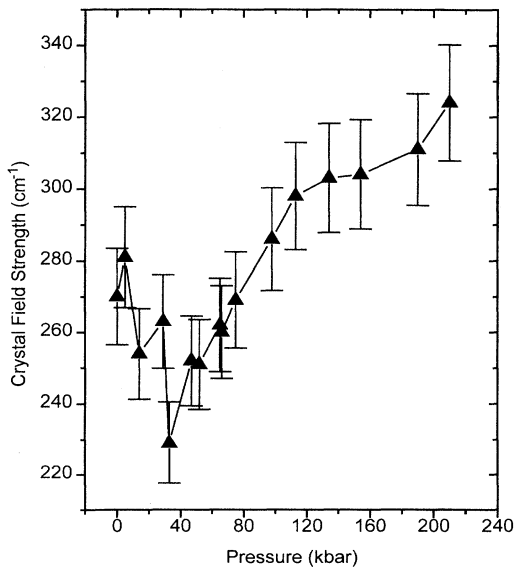

FIG. 7. Overall scalar crystal-field strength $S_{CF}^{(2)}$ [Eq. (4)] as a function of pressure. The values were derived from spectra generated by excitation of the peak of the $^5D_0 \leftarrow {}^7F_0$ band, which shifts to the red during compression.

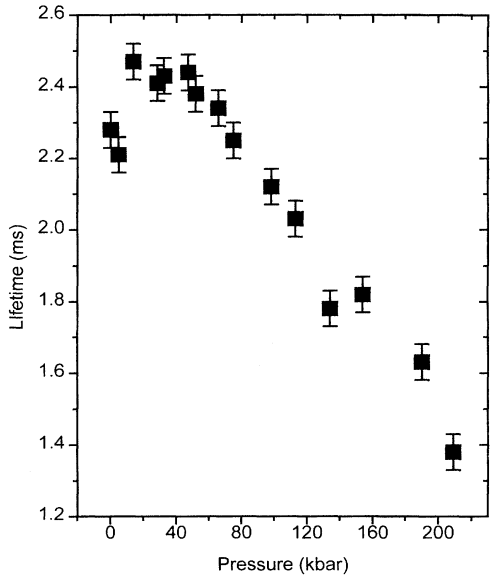

FIG. 8. Lifetimes of the $^5D_0$ state at 77 K as a function of pressure. Excitation wavelengths approximately follow the peak of the $^5D_0 \leftarrow {}^7F_0$ band: 0–33 kbar: $\lambda_{ex}=579$ nm. 47–210 kbar: $\lambda_{ex}=580$ nm. $^5D_0 \rightarrow {}^7F_2$ fluorescence was detected at 612 nm. Lifetimes of the slightly nonexponential decays were determined by integrating the area of the normalized decay curves.

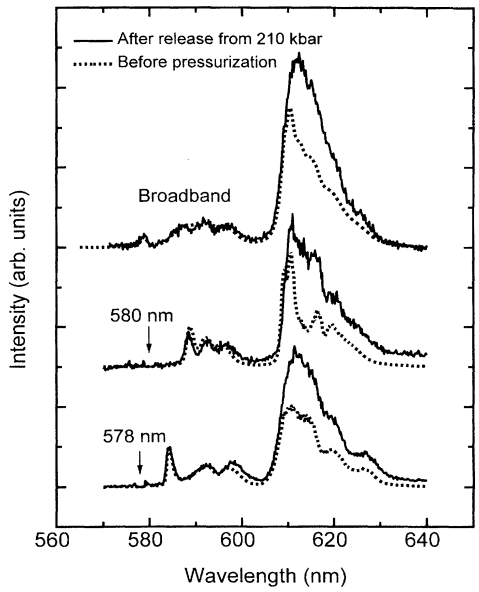

FIG. 9. Ambient-pressure broadband and FLN spectra before compression to 210 kbar (dashed curve) and after pressure release (solid curve). Broadband spectra were measured at 300 K and $\lambda_{ex}=465.8$ nm. FLN spectra were measured at 77 K and $\lambda_{ex}=578$ and 580 nm, as indicated on the plot. Spectra are normalized to the $^5D_0 \rightarrow {}^7F_1$ peak intensity.

ions in inorganic glasses and that "it is the overall electrostatic and covalent energy of the individual sites together with the site-to-site variation of this energy which hold the greatest influence." We believe these two factors, overall electrostatic energy and overall covalent energy, are linked to two experimental parameters. Specifically, we assess the overall electrostatic energy of the Eu^{3+} bonding environment with the field strength parameter S_{CF}, and we assess overall Eu-O bond covalency with the energy of the $^5D_0 \leftarrow {}^7F_0$ transition according to the nephelauxetic effect.[67]

It is important to note that we restrict the nephelauxetic effect analysis to compositionally similar modified silicate glasses or to different sites within a single glass. The review by Antic-Fidencev *et al.*[68] shows clearly that the $^5D_0$ state of Eu^{3+} shows little or no correlation with parameters such as bond length and coordination number when a variety of crystalline hosts are compared. We recognize concerns raised by these observations, but believe using the $^5D_0 \leftarrow {}^7F_0$ transition energy to assess overall Eu-O bond covalency is reasonable in our case, since both the nature of the ligands and the local structure are expected to vary gradually and continuously over different sites within a particular silicate glass. According to the nephelauxetic effect, therefore, we associate the low-energy side of the inhomogeneously broadened $^5D_0 \leftarrow {}^7F_0$ band with a more covalent Eu-O environment and the high-energy side of the band with a less covalent Eu-O environment.

The correlation between Eu^{3+}-site crystal-field strength and the $^5D_0 \leftarrow {}^7F_0$ band energy in silicate glasses is well established. Figure 6 shows that high-energy $^5D_0 \leftarrow {}^7F_0$ bands are linked to high-field-strength bonding sites and low-energy $^5D_0 \leftarrow {}^7F_0$ bands are linked to low-field-strength sites. The same trend can be seen in Fig. 6 of the simulated glass study of Cormier *et al.*,[52] and similar crystal-field strength conclusions were drawn by Brecher and Riseberg[58] nearly 20 years ago.

A third feature of the inhomogeneously broadened $^5D_0 \leftarrow {}^7F_0$ band is the variation of the observed fluorescence lifetime when different parts of the band are excited. Our results showed slight lengthening of the lifetimes as $^5D_0 \leftarrow {}^7F_0$ excitation was scanned from high to low energy (Table I). This effect was also demonstrated by Brecher and Riseberg.[58]

In summary, several overall trends are observed as the excitation wavelength is scanned across the inhomogeneously broadened $^5D_0 \leftarrow {}^7F_0$ band in silicate glasses. The high-energy (short-wavelength) side of the band represents the high-field sites where bonding is less covalent and the lifetimes are relatively short. The low-energy (long-wavelength) side of the band represents the low-field sites where bonding is more covalent and the lifetimes are relatively long. The issue to be resolved is what local structure features best explain these observed variations.

An important concept for understanding local Eu^{3+} structure in silicate glasses is the nonbridging oxygen (NBO) concentration in the material. NBO's are covalently bonded to one Si atom (Si-O^-) rather than the two Si atoms (Si-O-Si) linked by bridging oxygens (BO's). NBO's are formed in a silicate glass through the incorporation of basic oxides such as Na_2O or CaO in the glass matrix. Classic modifier cations such as Na^+ depolymerize the silicate matrix through the formation of NBO's.[69] The depolymerization has two primary effects. First, because the ionic interaction between Na^+ and the NBO is weak, NBO's carry more negative charge and are more polarizable than BO's. Second, local

network flexibility is increased because the NBO has one, rather than two, directional covalent Si-O bond. Several conclusions regarding Eu^{3+} local structure and optical properties can be explained in terms of the local NBO concentration around Eu^{3+}.

Because of their increased partial charge and polarizability, NBO's form more covalent bonds with Eu^{3+}, leading to a redshift of the $^5D_0 \leftarrow {}^7F_0$ band. This effect can be considered in terms of the optical basicity concepts outlined by Duffy and Ingram.[70] As the concentration of a basic oxide such as Na_2O is increased in silicate glass, the overall basicity of the glass is increased and the concentration of NBO's is increased. NBO's have a higher microscopic basicity than BO's, and as a result, Eu-O bonds are more covalent when the oxygens are nonbridging. Experimental evidence of the redshift of the $^5D_0 \leftarrow {}^7F_0$ band with increasing Na_2O concentration was presented by Todoroki *et al.*[71]

Given the observation that an overall increase in the Na_2O concentration shifts the $^5D_0 \leftarrow {}^7F_0$ band to the red, it is reasonable to conclude that within an inhomogeneously broadened $^5D_0 \leftarrow {}^7F_0$ band of a particular silicate glass, the low-energy (red) side of the band corresponds to sites with a high local NBO concentration. This result allows conclusions about the local bonding environment to be drawn. Eu^{3+} ions are generally associated with high coordination numbers. It has been argued that rare-earth ions exercise a degree of control over their own bonding environment in glasses and, in doing so, form quasimolecular complexes by forcing ligands into a "desired" bonding environment.[60] As concluded by Belliveau and Simkin, this process is more effective in the presence of a high local concentration of NBO's.[60] This implies that at sites with a large local NBO concentration Eu^{3+} ions can more effectively satisfy their high coordination requirements.

This conclusion is consistent with the recent EXAFS results of Ponader and Brown.[72] In that study, average Gd-O bond lengths were determined for albite, peralkaline, and sodium trisilicate glasses (note that Gd^{3+} and Eu^{3+} should have similar chemical properties). The glass with the highest theoretical NBO concentration in their study (sodium trisilicate) showed the longest Gd-O bond lengths and highest coordination numbers ($r=2.43$ Å, CN=8, respectively), which is consistent with the conclusion that rare-earth ions can more effectively satisfy their high-coordination-number requirements in glasses with high local NBO concentrations. Similar results were observed in the simulations of Cormier *et al.*,[73] where the theoretical NBO concentration was increased by adding Na_2O. The simulated Eu^{3+}-doped sodium disilicate glass showed longer average bond lengths and higher average coordination numbers ($r=2.60$ Å, CN=5.92) than the unmodified Eu^{3+}-doped silica glass ($r=2.49$ Å, CN =4.20).

These results can be used to conclude that on the average, the redshifted, low-crystal-field-strength Eu^{3+} sites in oxide glasses are characterized by a relatively large coordination number of NBO's.

Continuing with these arguments, it can be concluded that the high-field sites in silicate glasses probably consist of a lower local concentration of NBO's. Since fewer coordinating NBO's implies a less covalent Eu-O coordination sphere, the $^5D_0 \leftarrow {}^7F_0$ band associated with the high-field sites should be blueshifted. The study of Todoroki *et al.* shows a blueshift of the $^5D_0 \leftarrow {}^7F_0$ band in silicate glasses as the Na_2O concentration is decreased or as the Al_2O_3 concentration is increased, both of which lead to a decrease in the NBO concentration in the material.[71] There is no consensus on the description of the local bonding environment of Eu^{3+} at the high-field sites in silicate glasses. Brecher and Riseberg's model accounts for the observed crystal-field-strength increase by gradually increasing the oxygen coordination number from 8 to 9 with a simultaneous lengthening of bond lengths.[58] Similarly, Mössbauer studies by Tanabe *et al.* of the Eu_2O_3-Al_2O_3-SiO_2 system suggest large coordination numbers (8–12) in glasses with high-field-strength Eu^{3+} sites.[74]

Contrary to these high-coordination-number models are the results of the simulations of Cormier *et al.*[73] and Ponader and Brown's EXAFS studies.[72] These results show that in the silicate glasses with low theoretical NBO concentrations and high-field-strength bonding sites, shorter bond lengths and lower coordination numbers are, on the average, observed. The question to be answered is whether the high-field-strength sites in silicate glasses have large or small coordination numbers and long or short Eu-O bond lengths. HPFLN results shed light on this subject.

B. HPFLN

We divide the discussion of the high-pressure results into two pressure regimes: the initial-pressure regime (ambient pressure to ~40 kbar) and the high-pressure regime (~40–210 kbar).

1. Initial-pressure regime: Ambient pressure to 40 kbar

The initial-pressure regime is characterized by the simultaneous observation of a redshift of the $^5D_0 \leftarrow {}^7F_0$ band (Fig. 4), an overall crystal-field strength decrease (Fig. 7), and a lengthening of the fluorescence lifetimes (Fig. 8). A redshift of fluorescence bands with increasing pressure is not unexpected, given that the covalent character of the Eu-O bonds is expected to increase as bonds are shortened with compression. The relationship between pressure and field strength, however, is less predictable. For example, the overall field strength in Eu^{3+}:LaOCl and Eu^{3+}:LaOBr crystals is decreased with increasing pressure,[5,75] a result consistent with the initial pressurization of our glass sample. Eu^{3+}:Y_2O_2S and Eu^{3+}:La_2O_2S, however, show increased field strengths with increasing pressure.[76] While the analogy to field strengths in Eu^{3+}-doped crystal is largely inconclusive, we note that much larger $^5D_0 \leftarrow {}^7F_0$ redshifts are observed in the crystals that show a decrease in S_{CF} with pressure, an effect consistent with our observed redshift coincident with the decrease in S_{CF}.

The increase in the observed fluorescence lifetime is empirically consistent with the observed decrease in the crystal-field strength. As was noted earlier for the ambient-pressure silicate glasses, within an inhomogeneously broadened $^5D_0 \leftarrow {}^7F_0$ band, high-field strength sites are associated with short lifetimes and low-field strength sites are associated with long lifetimes.[58] As pressure to 40 kbar decreases the field strength, the observed lifetime increase is consistent with ambient-pressure observations.

Two physical effects could lead to longer lifetimes: a decrease in the nonradiative decay rate or a decrease in the radiative decay rate. Previous studies of Eu^{3+}-doped oxide glasses have reported quantum efficiencies close to unity at ambient pressure,[58] implying that nonradiative decay is negligible. The fact that our ambient-pressure lifetimes do not significantly vary between 300 and 77 K supports the conclusion that nonradiative decay effects are small. The observed lifetime at ambient pressure therefore approximates the radiative lifetime. The lifetime lengthening during pressurization, therefore, most likely reflects the radiative decay rate. In the absence of nonradiative decay effects, the lifetime of the $^5D_0$ state is determined largely by symmetry. Intraconfigurational f-f forced electric-dipole transitions are strictly forbidden in sites with inversion symmetry and gain intensity through admixture of opposite-parity states.[77] It is possible that a small local structural rearrangement towards centrosymmetry occurs between 0 and 40 kbar. An alternative explanation is decreased admixture of opposite-parity d states in this initial-pressure range. Both the symmetry and decreased admixture effects would decrease the radiative transition probabilities, leading to longer lifetimes. The latter explanation is particularly attractive given recent high-pressure studies[78,79] of crystals containing Sm^{2+}, which is isoelectronic with Eu^{3+}. These studies show that pressure increases the energy of the $4f^5 5d^1$ state relative to the $^5D_0$ state, resulting in sharp $^5D_0 \leftarrow {}^7F_J$ fluorescence. Since f-f transitions are forbidden by the parity selection rule, low transition probabilities (long lifetimes) are expected. Although the $4f^5 5d^1$ states in Eu^{3+} are higher in energy than they are in divalent Sm^{2+}, a pressure-induced energy increase would nevertheless decrease the d-state admixture with the emitting $^5D_0$ state, which could explain the observed lifetime lengthening.

The observations in the initial-pressure regime are used to conclude that only minor structural changes take place between ambient pressure and 40 kbar. Simple distortions of the Si-O-Si intertetrahedral angles are the most likely changes.[50] The lack of significant $^5D_0 \leftarrow {}^7F_0$ linewidth broadening in the initial-pressure regime also supports the conclusion that only minor structural modifications occur. We conclude that between ambient pressure and 40 kbar, overall Eu-O bond covalency is increased and small matrix modifications lead to slight Eu^{3+}-site symmetry changes. It is also possible that these pressures increase higher-lying d-state energies relative to the f states. In general, however, local structure modifications in the initial-pressure regime are small.

2. High-pressure regime: 40–210 kbar

At approximately 40 kbar, several of the trends observed in the initial-pressure regime reverse direction and new behavior is observed. These results suggest more profound local structural changes in the material. As pressure is increased above 40 kbar, simultaneous increases in the overall crystal-field strength (Fig. 7) and $^5D_0 \leftarrow {}^7F_0$ linewidth (Fig. 4) are observed along with a shortening of the fluorescence lifetimes (Fig. 8). Also note that between 40 and 150 kbar, minimal $^5D_0 \leftarrow {}^7F_0$ shifting is observed (Fig. 4). The fact that no $^5D_0 \leftarrow {}^7F_0$ shift occurs in this range suggests that high-field Eu^{3+} sites are being created with pressure. Since we expect high-field sites to appear on the high-energy (blue) side of the $^5D_0 \leftarrow {}^7F_0$ band, their creation opposes the red-shift observed in the initial pressure regime, and as a result, the $^5D_0 \leftarrow {}^7F_0$ broadens significantly, but does not shift. Consistent with the proposed formation of high-field sites is the observed increase in the overall field strength parameter S_{CF} with pressure above 40 kbar. A mechanism for the formation of high-field sites is discussed below.

As mentioned in the Introduction, the effect of pressure on silicate glass structure has been studied by a number of techniques. One of the main conclusions is that as pressure is increased, Si undergoes a gradual coordination change to five- and six-coordinate species.[34,37,39–42,49,50] A proposed mechanism for this coordination change in modified silicate glasses is that the Si coordination number is increased through consumption of NBO's, lowering the overall NBO concentration.[37] By analogy with the ambient-pressure glasses, a decrease in the NBO concentration should lead to an increase in the Eu^{3+}-site crystal-field strength and a blue-shift or broadening of the $^5D_0 \leftarrow {}^7F_0$ band. As mentioned in the previous paragraph, these phenomena are observed in the HPFLN spectra and spectral parameters. Therefore, our spectroscopic results are consistent with the expected Si coordination changes.

Another feature of the HPFLN spectra is that as pressure is increased, the fluorescence bands lose definition and different excitation wavelengths yield similar FLN spectra. We attribute this observation to a pressure-induced increase in the homogeneous linewidths associated with a given Eu^{3+} ion. Avouris *et al.*[80] and Morgan *et al.*[81] have shown that increased crystal-field strengths lead to increased homogeneous linewidths. Since pressures above 40 kbar progressively increase the crystal-field strengths, increased homogeneous linewidths are expected. This effect is manifested in increased linewidths at high pressure and decreased site selectivity, since a larger subset of sites is excited by the laser when large homogeneous linewidths overlap.

Avouris *et al.* argue that the increased homogeneous linewidth associated with increased crystal-field strength is the result of increased electron-phonon coupling at the high-field sites.[80] This conclusion is supported by our high-pressure fluorescence lifetime data. As seen in Fig. 8, when the pressure is increased above 40 kbar, the lifetimes progressively shorten. The observed behavior is interpreted in terms of an increase in the nonradiative decay rate above 40 kbar. Below 40 kbar, the nonradiative decay rate is negligible and the lifetime is determined by the radiative decay phenomena discussed above. As pressure is increased, however, nonradiative decay becomes more important as evidenced by the simultaneous observation of shorter lifetimes and an overall decrease of fluorescence signal. The best explanation for this nonradiative decay is pressure-induced electron-phonon coupling to local vibrations.

It should be noted that increased coupling to local vibrations is expected for shorter Eu-O bonding. Since Eu-O bonds are expected to be shortened as pressure is increased, this result is consistent with expected high-pressure behavior. This result also leads to an important conclusion about the high-field sites in the ambient pressure glass. As described above, two general models have been proposed to describe the high-field sites: one with large coordination numbers

and longer Eu-O bonds, the other with low coordination numbers and shorter bonds. The HPFLN results in the high-pressure regime are more consistent with the latter description, where a small number of closely bonded oxygens define the high-field sites. Thus the HPFLN results are more consistent with the conclusions drawn in simulation[73] and EXAFS studies.[72]

We have concluded that a characteristic of the high-field Eu^{3+} sites in silicate glasses is a low local NBO concentration. In an effort to satisfy its overall electrostatic and covalent energy requirements, the Eu^{3+} ions draw the few available NBO's closer than they would be in the high coordination state. The result is a small number of short, covalent Eu-O bonds that provide the local vibrations that lead to the increased electron-phonon coupling and the short lifetimes. Despite the presence of these covalent bonds, however, the overall bonding environment is less covalent than at the low-field sites, since the remainder of the Eu^{3+} coordination sphere is comprised of long, ionic bonds to low-charge-density bridging oxygens. As a result, blueshifted $^5D_0 \leftarrow ^7F_0$ bands are associated with the high-field sites.

We again note that these conclusions represent a description of the average high- and low-field sites. Individual sites are expected to vary in their local geometry, and we do not attempt to create a unique structural model. We do, however, believe that the general trends observed in the FLN data at ambient and high pressure can be used to draw conclusions about the average local bonding environment.

C. Structural changes on pressure release

Previous studies of silica and silicate glasses quenched from high pressures have shown that irreversible structural changes occur even at room temperature.[37,82,83] Spectra in Fig. 9 show that the structure on pressure release is different from both the initial- and high-pressure structures. The short lifetimes observed on pressure release from 210 kbar initially suggest that residual high-pressure structure is maintained on pressure release. At high pressures, however, a low overall fluorescence signal was observed. The signal after pressure release returned to approximately its initial value. This suggests that the short lifetime on pressure release is not the result of nonradiative decay, but instead some structural effect on the radiative decay rate.

These spectroscopic results are consistent with the high-pressure Raman studies of Wolf *et al.*[37] These authors found that a final release structure in sodium tetrasilicate glass was formed not during compression, but during decompression.[37] Specifically, they state that the high coordinate Si species release to a different distribution of Q^n values resulting from disproportionation reactions. Such a structural change in the vicinity of a Eu^{3+} ion is manifested in alteration of the spectroscopic properties. Because of the high cation field strength of Eu^{3+}, it is plausible that the Eu^{3+} ion itself contributes to the disproportionation reactions. Both the increased hypersensitive $^5D_0 \rightarrow ^7F_2$ transition intensity and the short fluorescence lifetimes are suggestive of Eu^{3+} bonding sites that are more severely distorted (asymmetric) than those in the glass originally quenched from the melt at ambient pressure.

VI. CONCLUSION

High-pressure fluorescence line narrowing studies of Eu^{3+}-doped sodium disilicate glass have been carried out at hydrostatic pressures up to 210 kbar. The gradual evolution of the FLN spectra was consistent with the gradual structural changes expected to occur in silicate glasses with pressure. Increasing pressure to 40 kbar decreased the overall crystal-field strength at Eu^{3+} sites and lengthened the fluorescence lifetimes. Above 40 kbar, the effect of pressure was to increase the overall crystal-field strength and shorten the lifetimes. Pressure results were interpreted in terms of structural changes and increased electron-phonon coupling to local vibrational modes.

The results suggest that high-crystal-field Eu^{3+} sites in glass are associated with a low local concentration of nonbridging oxygens, low coordination numbers, and short Eu-O bonds. Conversely, weak field sites are characterized by a high local concentration of nonbridging oxygens, high coordination numbers, and long Eu-O bonds.

Given the correlation between crystal-field strength and fluorescence properties, the ability to tune crystal-field strength while maintaining a degree of site selectivity makes HPFLN spectroscopy a useful complement to existing techniques. HPFLN studies of different glass compositions will improve our understanding of high-pressure melts, which is critical to our understanding of Earth's chemical evolution. HPFLN studies will also improve our understanding of ambient-pressure optical device materials, since a new level of control over structural properties is provided.

ACKNOWLEDGMENT

Financial support from the National Science Foundation under Grant No. EAR-9311543 is gratefully acknowledged.

*Author to whom correspondence should be addressed: Kevin L. Bray, Department of Chemical Engineering, 1415 Johnson Dr., Madison, WI 53706; FAX (608)262-5434; electronic address: bray@engr.wisc.edu

[1] M. J. Weber, in *Laser Spectroscopy of Solids*, 2nd ed., edited by W. M. Yen and P. M. Selzer (Springer-Verlag, Berlin, 1986), p. 189.

[2] F. Durville, G. Boulon, R. Reisfeld, H. Mack, and C. K. Jørgensen, Chem. Phys. Lett. **102**, 393 (1983).

[3] J. A. Capobianco, T. F. Belliveau, G. Lord, D. J. Simkin, J. Tait, and P. J. Howard, Phys. Rev. B **34**, 4204 (1986).

[4] H. G. Drickamer and C. W. Frank, *Electronic Transitions and the High Pressure Chemistry and Physics of Solids* (Chapman-Hall, London, 1973).

[5] Q. Wang and A. Bulou, Solid State Commun. **94**, 309 (1995).

[6] Q. Wang, L. Lun, D. Zhang, Y. Chi, and L. Wang, J. Phys. Condens. Matter **4**, 6491 (1992).

[7] J. F. Dolan, L. A. Kappers, and R. H. Bartram, Phys. Rev. B **33**, 7339 (1986).

[8] D. Ma, Z. Wang, J. Chen, and Z. Zhang, J. Phys. C **21**, 3585 (1988).

[9] U. Hömmerich and K. L. Bray, Phys. Rev. B **51**, 12 133 (1995).

[10] U. Hömmerich and K. L. Bray, Phys. Rev. B **51**, 8595 (1995).
[11] P. T. C. Friere, O. Pilla, and V. Lemos, Phys. Rev. B **49**, 9232 (1994).
[12] D. Galanciak, P. Perlin, M. Grinberg, and A. Suchocki, J. Lumin. **60 & 61**, 223 (1994).
[13] A. G. Rinzler, J. F. Dolan, L. A. Kappers, D. S. Hamilton, and R. H. Bartram, J. Phys. Chem. Solids **54**, 89 (1993).
[14] J. F. Dolan, A. G. Rinzler, L. A. Kappers, and R. H. Bartram, J. Phys. Chem. Solids **53**, 905 (1992).
[15] P. R. Wamsley and K. L. Bray, J. Lumin. **59**, 11 (1994).
[16] P. R. Wamsley and K. L. Bray, J. Lumin. **63**, 31 (1995).
[17] A. H. Jahren, M. B. Kruger, and R. Jeanloz, J. Appl. Phys. **71**, 1579 (1992).
[18] S. J. Duclos, Y. K. Vohra, and A. L. Ruoff, Phys. Rev. B **41**, 5372 (1990).
[19] T. Tröster, T. Gregorian, and W. B. Holzapfel, Phys. Rev. B **48**, 2960 (1993).
[20] Y. R. Shen and W. B. Holzapfel, Phys. Rev. B **51**, 15 752 (1995).
[21] Y. R. Shen and W. B. Holzapfel, Phys. Rev. B. **51**, 6127 (1995).
[22] G. Chen, S. Wang, R. G. Haire, and J. R. Peterson, Appl. Spectrosc. **48**, 1026 (1994).
[23] H. Yusa, T. Yagi, and H. Arashi, J. Appl. Phys. **75**, 1463 (1994).
[24] N. J. Hess and D. Schiferl, J. Appl. Phys. **68**, 1953 (1990).
[25] G. Chen, R. G. Haire, J. R. Peterson, and M. M. Abraham, J. Phys. Chem. Solids **55**, 313 (1994).
[26] G. Changxin, L. Bilin, H. Yuefen, and C. Hongbin, J. Lumin. **48 & 49**, 489 (1991).
[27] S. Liu, Y. Chi, and L. Wang, J. Lumin. **40 & 41**, 395 (1988).
[28] G. Webster and H. G. Drickamer, J. Chem. Phys. **72**, 3740 (1980).
[29] G. Huber, K. Syassen, and W. B. Holzapfel, Phys. Rev. B **15**, 5123 (1977).
[30] G. Chen, N. A. Stump, R. G. Haire, and J. R. Peterson, Solid State Commun. **89**, 1005 (1994).
[31] R. E. Tischer, J. Chem. Phys. **48**, 4291 (1968).
[32] R. E. Tischer and H. G. Drickamer, J. Chem. Phys. **37**, 1554 (1962).
[33] N. Soga, K. Hirao, M. Yoshimoto, and H. Yamamoto, J. Appl. Phys. **63**, 4451 (1988).
[34] Q. Williams, R. J. Hemley, M. B. Kruger, and R. Jeanloz, J. Geophys. Res. **98**, 22 157 (1993).
[35] J. D. Kubicki, R. J. Hemley, and A. M. Hofmeister, Am. Mineral. **77**, 258 (1992).
[36] R. J. Hemley, H. K. Mao, P. M. Bell, and B. O. Mysen, Phys. Rev. Lett. **57**, 747 (1986).
[37] G. H. Wolf, D. J. Durban, and P. F. McMillan, J. Chem. Phys. **93**, 2280 (1990).
[38] S. K. Sharma, T. F. Cooney, and S. Y. Wang, J. Non-Cryst. Solids **179**, 125 (1994).
[39] J. F. Stebbins and P. McMillan, Am. Mineral. **74**, 965 (1989).
[40] X. Xue, J. F. Stebbins, M. Kanzaki, and R. G. Trønnes, Science **245**, 962 (1989).
[41] X. Xue, J. F. Stebbins, M. Kanzaki, P. F. McMillan, and B. Poe, Am. Mineral. **76**, 8 (1991).
[42] X. Xue, J. F. Stebbins, and M. Kanzaki, Am. Mineral. **79**, 31 (1994).
[43] C. Meade, R. J. Hemley, and H. K. Mao, Phys. Rev. Lett. **69**, 1387 (1992).
[44] C.-S. Zha, R. J. Hemley, H. K. Mao, T. S. Duffy, and C. Meade, Phys. Rev. B **50**, 13 105 (1994).
[45] R. G. Burns, *Mineralogical Applications of Crystal Field Theory*, 2nd ed. (Cambridge University Press, Cambridge, England, 1993).
[46] R. M. Abu-Eid, in *The Physics and Chemistry of Minerals and Rocks*, edited by R. G. J. Strens (Wiley, New York, 1976).
[47] H. G. Smith and K. Langer, Am. Mineral. **67**, 343 (1982).
[48] D. M. Sherman, Adv. Geochem. **7**, 113 (1988).
[49] Q. Williams and R. Jeanloz, Science **239**, 902 (1988).
[50] E. M. Stolper and T. J. Ahrens, Geophys. Res. Lett. **14**, 1231 (1987).
[51] R. Jeanloz, Nature **332**, 207 (1988).
[52] G. Cormier, J. A. Capobianco, C. A. Morrison, and A. Monteil, Phys. Rev. B **48**, 16 290 (1993).
[53] R. A. Forman, G. J. Piermarini, J. D. Barnett, and S. Block, Science **176**, 284 (1972).
[54] G. J. Piermarini, S. Block, and J. D. Barnett, J. Appl. Phys. **44**, 5377 (1973).
[55] B. G. Wybourne, *Spectroscopic Properties of Rare Earths* (Interscience, New York, 1965).
[56] C. A. Morrison and R. P. Leavitt, in *Handbook on the Physics and Chemistry of Rare Earths*, edited by K. A. Gschneider and L. Eyring (North-Holland, Amsterdam, 1982), Vol. 5, p. 461.
[57] A. Lempicki, H. Samelson, and C. Brecher, J. Mol. Spectrosc. **27**, 375 (1968).
[58] C. Brecher and L. A. Riseberg, Phys. Rev. B **13**, 81 (1976).
[59] P. Porcher and P. Caro, J. Lumin. **21**, 207 (1980).
[60] T. F. Belliveau and D. J. Simkin, J. Non-Cryst. Solids **110**, 127 (1989).
[61] F. Auzel, Mater. Res. Bull. **14**, 223 (1979).
[62] F. Auzel and O. L. Malta, J. Phys. (Paris) **44**, 201 (1983).
[63] R. P. Leavitt, J. Chem. Phys. **77**, 1661 (1982).
[64] N. C. Chang, J. B. Gruber, R. P. Leavitt, and C. A. Morrison, J. Chem. Phys. **76**, 3877 (1982).
[65] J. Dexpert-Ghys, B. Pirou, N. Jacquet-Francillon, and C. Sombret, J. Non-Cryst. Solids **125**, 117 (1990).
[66] M. J. Weber and S. A. Brawer, J. Non-Cryst. Solids **52**, 321 (1982).
[67] C. K. Jørgensen, Prog. Inorg. Chem. **4**, 73 (1962).
[68] E. Antic-Fidancev, M. Lemaitre-Blaise, and P. Caro, New J. Chem. **11**, 467 (1987).
[69] H. Scholze, *Glass: Nature, Structure and Properties* (Springer-Verlag, New York, 1991).
[70] J. A. Duffy and M. D. Ingram, J. Non-Cryst. Solids **21**, 373 (1976).
[71] S. Todoroki, K. Hirao, and N. Soga, J. Appl. Phys. **72**, 5853 (1992).
[72] C. W. Ponader and G. E. Brown, Jr., Geochim. Cosmochim. Acta **53**, 2893 (1989).
[73] G. Cormier, J. A. Capobianco, and A. Monteil, J. Non-Cryst. Solids **152**, 225 (1993).
[74] S. Tanabe, K. Hirao, and N. Soga, J. Non-Cryst. Solids **113**, 178 (1989).
[75] Y. Chi, S. Liu, W. Shen, L. Wang, and G. Zou, Physica **139 & 140B**, 555 (1986).
[76] Q. Wang, L. Lun, D. Zhang, Y. Chi, and L. Wang, J. Phys. Condens. Matter **4**, 6491 (1992).
[77] R. D. Peacock, Struct. Bonding (Berlin) **22**, 83 (1975).
[78] C. S. Yoo, H. B. Radousky, N. C. Holmes, and N. M. Edelstein, Phys. Rev. B **44**, 830 (1991).

[79] G. Chen, S. Wang, R. G. Haire, and J. R. Peterson, Appl. Spectrosc. **48**, 1026 (1994).
[80] P. Avouris, A. Campion, and M. A. El-Sayed, J. Chem. Phys. **67**, 3397 (1977).
[81] J. R. Morgan, E. P. Chock, W. D. Hopewell, M. A. El-Sayed, and R. Orbach, J. Phys. Chem. **85**, 747 (1981).
[82] P. W. Bridgman and I. Simon, J. Appl. Phys. **24**, 405 (1953).
[83] R. Roy and H. M. Cohen, Nature **190**, 798 (1961).